Theoretical Investigation of a Water-Gas-Shift Catalytic Membrane for Diesel Reformate Purification

Bhanu Vardhan Reddy Kuncharam and Benjamin A. Wilhite
Artie McFerrin Dept. of Chemical Engineering, Texas A&M University, College Station, TX 77843

DOI 10.1002/aic.14188
Published online July 30, 2013 in Wiley Online Library (wileyonlinelibrary.com)

The novel application of a catalytic water-gas-shift membrane reactor for selective removal of CO from H_2-rich reformate mixtures for achieving gas purification solely via manipulation of reaction and diffusion phenomena, assuming Knudsen diffusion regime and the absence of hydrogen permselective materials, is described. An isothermal, two-dimensional model is developed to describe a tube-and-shell membrane reactor supplied with a typical reformate mixture (9% CO, 3% CO_2, 28% H_2, and 15% H_2O) to the retentate volume and steam supplied to the permeate volume such that the overall H_2O:CO ratio within the system is 9:1. Simulations indicate that apparent CO:H_2 selectivities of 90:1 to >200:1 at H_2 recoveries of 20% to upwards of 40% may be achieved through appropriate design of the catalytic membrane and selection of operating conditions. Under these conditions, simulations predict an apparent hydrogen permeability of 2.3×10^{-10} mol m^{-1} Pa, which compares favorably against that of competing hydrogen-permselective membranes. © 2013 American Institute of Chemical Engineers *AIChE J*, 59: 4334–4345, 2013
Keywords: catalytic membrane reactor (CMR), gas purification, membrane separations, reactor analysis, mathematical modeling

Introduction

The development of cost-effective hydrogen purification technologies remains a critical challenge to the modern petrochemical industry,[1,2] owing to its many uses in the refinery, from treating sour crude oils to catalytic upgrading of olefins.[1,3] The growth of the biorefinery industry for producing alternative fuels from domestic and renewable resources is expected to increase hydrogen demand, as current biofuels require significant upgrading and reforming to achieve combustion properties comparable to petroleum distillates.[4,5] Likewise, demand for hydrogen in the petrochemical industry is expected to continue to rise as increasingly sulfur- and nitrogen-rich crude oils populate the market.[2]

Steam reforming of hydrocarbons, which yields a hydrogen-rich gas mixture containing significant amounts of both carbon monoxide and carbon dioxide, represents 95% of total hydrogen production.[6,7] Subsequent hydrogen purification can be achieved through cryogenic distillation, absorption, pressure-swing adsorption, or membrane separation, with the latter being of particular interest owing to the combination of low maintenance and operating costs, continuous operation, and high capacities.[8–10] Existing permselective membrane technologies reported in the literature to-date for hydrogen purification have primarily used either permselective polymeric[11–13] or palladium-based[14] materials. In both cases, additional hydrogen recovery from reformate mixtures has been demonstrated by coupling the permselective membrane with water-gas-shift reaction.[15,16] Polymeric membranes provide promising permselectivities (typically 50–100:1) between hydrogen and carbon monoxide at relatively low costs, but lack thermal stability at temperatures above 200°C which limits their compatibility with high-temperature water-gas-shift reaction or other supporting catalytic reactions.[17,18] Dense palladium membranes present infinite theoretical permselectivity for hydrogen over any other gaseous species,[14] but lose permeability when exposed to steam and carbonaceous species owing to competitive surface adsorption[19–21] and are prone to embrittlement after several thermal and H_2 exposure cycles.[14,22] These issues with palladium membranes can be mitigated by alloying with metals such as Ag, Cu, Au, and Ru,[14] or by operation at sufficiently high temperatures as to minimize competitive adsorption effects. Microporous inorganic membranes (pore size <1 nm) have also been successfully used for selective hydrogen separation.[23,24] These membranes are primarily silica-based, which can be easily produced using either sol-gel dip coating or chemical vapor deposition[23,25] and have shown to yield H_2/N_2 selectivity exceeding 10,000.[26] However, they have poor chemical stability when exposed to water vapor which is either a product or a reactant in hydrocarbon reforming.[25] Although the above permselective membrane technologies have been directed at achieving high-purity hydrogen (>99.9% H_2), in many industrial applications hydrogen purity requirements are far less stringent, with the majority of refinery operations requiring hydrogen purities of 80–95%.[1–3] This then makes the selective removal of carbon monoxide the primary objective for hydrogen purification for industrial applications.

In this article, the authors explore the use of a nonpermselective catalytic membrane reactor (CMR) to achieve competitive carbon monoxide removal from hydrogen-rich reformate

Correspondence concerning this article should be addressed to B. A. Wilhite at benjaminwilhite@mail.che.tamu.edu.

mixtures via water-gas-shift reaction, while avoiding the costs and limitations associated with polymeric or metallic permselective materials. Catalytic membrane reactors, in which a porous, nonpermselective catalytically active membrane provides simultaneous reaction and separation between two distinct flow volumes, have been successfully used to address multiple chemical reactor design challenges to-date.[27,28] Flow-through catalytic membrane reactors,[28] in which all reactants are forced to transport through the catalytic membrane, have been investigated for achieving moderate separation of reaction products owing to disparities in species diffusivities[29,30] which can be further exploited to overcome equilibrium limitations on reaction conversion.[28,31]

Segregation of reactants between either face of the catalytic membrane enables greater manipulation of reaction selectivity,[31–33] by exploiting the diffusional resistances within the membrane to control the extent of reagent mixing. In the limit of complete segregation of reactants and sufficient membrane thickness, the catalytic membrane effectively prevents crossover or "slip" of the segregated reactants from one fluid volume to the other.[34–36] This approach to catalytic membrane reactor design was first proposed by Sloot et al.[34] for the case of the Claus reaction between hydrogen sulfide and sulfur dioxide, in which the counterdiffusion profile of reactants combined with significant diffusional resistances resulted in almost complete prevention of reactant crossover. Subsequent investigations have further demonstrated the value of this approach for carrying out processes normally requiring strict stoichiometric feed rates of reactants, or in which crosscontamination of reactants is undesirable.[31,35]

In this work, the authors explore the extension of the above membrane reactor concepts to the task of carbon monoxide removal from hydrogen mixtures using a catalytic membrane active for water-gas-shift reaction. This represents the first exploration of employing catalytic membrane reactors in the absence of any permselective materials (barring permselectivities arising from Knudsen diffusion), for the purpose of gas purification. In lieu of permselective materials (e.g., palladium), water-gas-shift reaction is used to convert CO contaminant to a combination of desired hydrogen and benign carbon dioxide by-product, while supply of additional steam coreactant to the permeate surface provides a means to overcome equilibrium limitations of carbon monoxide conversion within the membrane. In doing so, this effort establishes a tradeoff between maximizing hydrogen permeance across the membrane and minimizing "slip" of carbon monoxide contaminant. This is achieved by using a combination of intermediate membrane thicknesses and the addition of steam coreactant to the permeate volume. The ability to achieve selective gas purification in the absence of any permselective materials is explored through a series of two-dimensional (2-D) design simulations of this catalytic membrane concept over a range of catalytic membrane activity, thickness, and operating temperature. Results demonstrate the potential of combining the principles of flow-through and segregated-flow catalytic membrane reactors to achieve gas purification without permselective materials.

Theoretical

Design of catalytic membrane reactor for CO removal from reformates

A countercurrent shell-and-tube catalytic membrane system is proposed for the present theoretical investigation (Figure 1a). The tubular membrane itself may be formed from a macroporous mechanical support of sufficient thickness using established sol-gel[37] techniques in conjunction with vacuum-infiltration to ensure the macropore network of the mechanical support is loaded with active material. Alternately, deposition of the catalytic layer overtop the mechanical support may be achieved via washcoating methods.[38] The present model may be applicable to the latter case as well, assuming negligible transport resistances within the macroporous substrate such that it may be effectively omitted.

A 2-D model is developed to describe the membrane reactor operating in countercurrent flow mode (Figure 1) with an inner or bore radius of 4.75 mm (based on a typical porous stainless steel substrate) and an outer or shell radius calculated based on the catalytic membrane thickness to ensure identical retentate and permeate flow volumes (see Figure 1b). Catalyst membrane thickness, t, and catalyst activity factor, δ, are selected such that CMR performance is investigated over a range of normalized Thiele modulus (Φ) and dimensionless separation factor (ξ). The catalyst activity factor represents the activity of the catalytic membrane relative to a reference material (in this study, the activity of a 5 wt % CuO/Al_2O_3 catalyst for which water-gas-shift kinetics are known).

The normalized Thiele modulus is determined from Eq. 1 using shape- and second-order kinetics normalizations following Aris[39] and accounting for reaction reversibility following Carberry[40]

$$\Phi = t_{\text{cat}} \left[\frac{r_o\left(p^F_{\text{CO},o}, T\right) \cdot \text{RT}}{D^{\text{eff}}_{\text{CO}} \cdot p^{\text{F}}_{\text{CO},o}} \right] \cdot \left(\frac{1}{2}\right) \cdot \left(\frac{2}{3}\right)^{1/2} \cdot \left(\frac{K_{\text{eq}}+1}{K_{\text{eq}}}\right)^{1/2} \tag{1}$$

The resulting design parameter represents a dimensionless ratio of the rate of CO reaction within the membrane relative to the permeation rate of CO (undesired permeate) across the membrane. A dimensionless separation factor, ξ, is then defined as the ratio of hydrogen (desired permeate) transport across the membrane relative to the rate of CO conversion by water-gas-shift reaction within the membrane, and is defined as

$$\xi = \frac{A_{\text{mem}}}{V_{\text{mem}}} \frac{\left(\frac{D^{\text{eff}}_{H_2}}{t_{\text{mem}}}\right)\left(\frac{p^{\text{F}}_{H_2,o}}{\text{RT}}\right)}{\eta_o \cdot \delta \cdot r_o\left(p_{i,o,}T\right)} \tag{2}$$

A summary of catalyst thicknesses and activity factors used in this work to investigate membrane designs spanning $\Phi \in (1..7.6)$ and $\xi \in (0.1..10)$ is provided in Table 1.

A simulated diesel reformate mixture comprised of 9% CO, 15% H_2O, 28% H_2, and 3% CO_2[41] is supplied to the retentate volume, whereas pure steam is supplied to the permeate volume as a sweep gas. The use of steam as sweep gas provides segregation of reactants for water-gas-shift across the catalytic volume such that slip of CO from retentate to permeate volume is minimized. The sweep gas flow rate is then determined such that an overall CO:H_2O molar supply ratio of 9:1 is maintained over all feed or reformate flow rates studied. For each value of feed or reformate flow rate, a dimensionless Damkohler number is calculated based on the initial rate of water-gas-shift reaction and residence time as follows

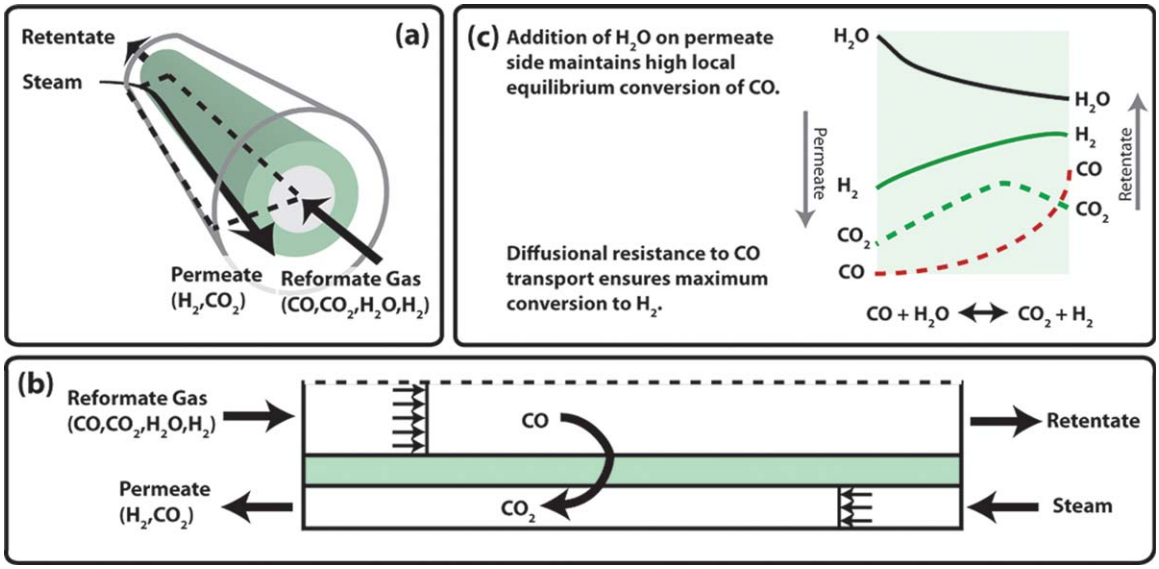

Figure 1. Water-gas-shift catalytic membrane for selective removal of carbon monoxide from hydrogen-rich reformate mixtures.

(a) Schematic of membrane operation; (b) cross-section of membrane highlighting modeling approach; (c) concentration profiles through radial cross-section of membrane illustrating principle for carbon monoxide removal. [Color figure can be viewed in the online issue, which is available at wileyonlinelibrary.com.]

$$\mathrm{Da} = \left(\frac{\eta(\Phi) \cdot \delta \cdot r_o\left(p^{\mathrm{F}}_{\mathrm{CO,o}}, T_o\right) \cdot \mathrm{RT}}{p^{\mathrm{F}}_{\mathrm{H_2,o}}} \right) \cdot \left(\frac{F^{\mathrm{F}}_{\mathrm{CO,o}}}{V^{\mathrm{F}}} \cdot \frac{\mathrm{RT}}{P} \right) \quad (3)$$

Performance of individual membrane designs is investigated by simulating each catalytic membrane reactor design over a broad span of Da to encompass both high apparent H_2:CO permselectivity and high H_2 recovery regimes.

Model assembly

A steady-state 2-D model is developed to describe the reaction, diffusion, and/or heat conduction within the catalytic membrane active for water-gas-shift reaction in catalytic membrane reactor architecture described above for both isothermal and adiabatic cases. Reaction and diffusion in the catalytic membrane is described assuming a nominal pore diameter of 10 nm and negligible transmembrane pressure drop (i.e., equal retentate and permeate pressures), such that a single-component Fick's diffusion model with effective Knudsen diffusivities may be used

$$\nabla\left(D^{\mathrm{eff}}_{K,i} \nabla C_i\right) = -r_i \cdot \delta \ \text{ where } C_i = \frac{P x_i}{\mathrm{RT}} \quad (4a)$$

Assuming a porosity of 45% and tortuosity of 2,[42] the effective Knudsen diffusivity is estimated from kinetic theory of gases

$$D^{\mathrm{eff}}_{k,i} = \frac{\varepsilon}{\tau}\left(\frac{1}{3} d_p \left[\frac{8\mathrm{RT}}{\pi \cdot M_i}\right]^{0.5}\right) \quad (4b)$$

Water-gas-shift reaction is modeled using the power-law rate expression described by Mizsey et al.[43] for a CuO/Al_2O_3 (5% copper on alumina) catalyst, assuming a catalyst density of 1000 kg m^{-3}

$$r_{\mathrm{CO}} = k_f\left(p^{\mathrm{cat}}_{\mathrm{CO}} p^{\mathrm{cat}}_{\mathrm{H_2O}} - \frac{p^{\mathrm{cat}}_{\mathrm{CO_2}} p^{\mathrm{cat}}_{\mathrm{H_2}}}{K_{\mathrm{eq}}}\right) \quad (5a)$$

with forward rate and equilibrium coefficients defined as

$$k_{\mathrm{f}} = 2.25\times10^{-3}\exp\left[\frac{-50,000}{\mathrm{RT}^{\mathrm{cat}}}\right] \text{ and } k_{\mathrm{eq}} = 9.543\times10^{-3}\exp\left[\frac{39,876}{\mathrm{RT}^{\mathrm{cat}}}\right] \quad (5b)$$

Retentate and permeate fluid volumes are modeled assuming ideal plug flow behavior with no axial dispersion or back mixing. Both volumes are assumed to be isobaric with uniform outlet pressure of 1 atm (i.e., assuming negligible pressure drop). The resulting 1-D equations describing individual species molar flow along the axial length of the membrane assume mass appearance in the bulk fluid volume occurs via gas-solid mass transfer, that is

$$\frac{1}{A^F_C}\frac{dF^F_i}{dz} = -k_{gs}\tilde{a}^F\left(p^F_i - p^{\mathrm{cat}}_i\right), F^F_i = F^F_{i,o} \ \ @z=0 \quad (6a)$$

$$-\frac{1}{A^S_C}\frac{dF^S_i}{dz} = -k_{gs}\tilde{a}^S\left(p^S_i - p^{\mathrm{cat}}_i\right), F^S_i = F^S_{i,o} \ \ @z=0.15 \quad (6b)$$

The fluid and catalyst volume models are linked through boundary conditions equating individual species mass fluxes normal to the fluid-catalyst boundary

$$\nabla\left(D^{\mathrm{eff}}_{K,i} C_i\right) \cdot \tilde{n} = \mathbf{k}_{gs}\left(p^{F,S}_i - p^{\mathrm{cat}}_i\right) \cdot M_i \quad (6c)$$

Table 1. Summary of Design Parameters Employed for Present Study

$\xi = 0.1$			$\Phi = 7.6$		
Φ	t (m)	δ	ξ	t (m)	δ
7.6	1.56×10^{-3}	0.23	0.1	1.56×10^{-3}	0.23
5.24	1.32×10^{-3}	0.15	0.2	1.13×10^{-3}	0.44
2.99	1.01×10^{-3}	0.086	0.3	0.93×10^{-3}	0.65
2.5	0.96×10^{-3}	0.077	0.4	0.81×10^{-3}	0.86
2.3	0.89×10^{-3}	0.065	0.5	0.73×10^{-3}	1.06
1.7	0.77×10^{-3}	0.048	1	0.52×10^{-3}	2.08
1.3	0.68×10^{-3}	0.036	2	0.37×10^{-3}	4.09
			5	0.24×10^{-3}	10.1
			10	0.17×10^{-3}	20.0

Initial analysis is performed assuming isothermal operation to isolate the impact of mass transport and reaction on membrane performance. Subsequent analysis is performed assuming adiabatic operation to investigate the impact of reaction heat on membrane performance. Conductive heat transport within the catalytic membrane is described using an effective thermal conductivity following Butt[44]

$$\nabla(k_{\text{cat}}\nabla T^{\text{cat}}) = \left(-\Delta H^{o}_{r\times n}\right)\cdot(-r_{\text{CO}}\cdot\delta) \tag{7a}$$

$$\text{where } k_{\text{cat}} = \varepsilon^2 k_{\text{gas}} + (1-\varepsilon)k_{\text{solid}} \tag{7b}$$

Fluid-phase energy balances assuming 1-D plug flow with heat appearance in bulk fluid occurring solely via gas-solid heat transfer are used with initial conditions corresponding to inlet retentate and sweep temperatures at $z = 0$ and $z = 0.15$, respectively

$$\frac{dT^F}{dz} = \left(\sum_{i=1}^{n} Cp_i \cdot F^F_{i,o}\right) h^F \cdot \hat{a}^F \cdot A^F_C\left(T^{\text{cat}} - T^F\right), \quad \text{I.C.}$$

$$T^F = T^F_o \ @z=0 \tag{8a}$$

$$-\frac{dT^F}{dz} = \left(\sum_{i=1}^{n} Cp_i \cdot F^S_{i,o}\right) h^S \cdot \hat{a}^S \cdot A^S_C\left(T^{\text{cat}} - T^S\right), \quad \text{I.C.}$$

$$T^S = T^S_o \ @\text{z}=0.15 \tag{8b}$$

The fluid-wall heat-transfer coefficient is estimated from the fluid Prandtl (Pr) and Reynolds numbers (Re) following Eq. 8c, valid at Reynolds numbers between 40 and 2000[45]

$$Nu_{fw} = \frac{h_{fs}d_p}{k_g} = (0.24)\text{Pr}^{\frac{1}{3}}\ \text{Re}^{0.8},\ \ \text{Re} = \left(\frac{d_t\rho\mu}{\mu_{\text{mix}}}\right), \text{Pr} = \frac{C_{P,\text{mix}}\,\mu_{\text{mix}}}{k_{\text{cat}}} \tag{8c}$$

Fluid velocity is calculated from the sum of individual species molar flow rates and assuming ideal gas relationship between molar and volumetric flow rates. Dynamic viscosity of the gas mixture is evaluated as a function of composition and temperature using the semiempirical formula developed by Wilke,[46] with all values for Lennard–Jones parameters taken from[47]

$$\mu = \sum_{i=1}^{n} \frac{x_i\mu_i}{x_i + \sum_{i=1}^{n} x_i\phi_{ij}},\ \ \text{where } \phi_{ij} = \frac{\left[1+\left(\frac{\mu_i}{\mu_j}\right)^{1/2}\left(\frac{M_j}{M_i}\right)^{1/4}\right]^2}{\sqrt{8}\cdot\left(1+\frac{M_i}{M_j}\right)^{1/2}}$$

$$\text{and } \mu_i = 2.67\times10^{-5}\frac{\sqrt{M_iT}}{\sigma^2\Omega_\mu} \tag{8d}$$

The fluid and solid-phase energy balances are coupled at the boundary of retentate and permeate volumes using Eq. 8a and 8b, solved with given initial conditions.

Numerical methods

The resulting 2-D model was implemented using the commercial COMSOL Multiphysics V3.5 environment equipped with the Chemical Engineering Module, using separate convection and conduction physics modules in 2-D radial symmetry mode to describe mass and heat transport within the catalyst volume. Separate coefficient-form partial differential equation modules are used to describe convective heat and mass transport in retentate and permeate volumes. Weak boundary form equations are used to describe the solid-fluid heat transfer at the boundaries. Finite element meshes used in this work consisted of approximately 30,000 triangular elements, resulting in $\sim 4 \times 10^5$ degrees of freedom. All numerical solutions met overall and atomic mass balances within 0.01% error. Further refinement in mesh size resulted in negligible change in solution accuracy. Solutions were obtained using the prepackaged stationary Direct UMFPACK solver (v4.2) written by Davis, who employs an unsymmetric multifrontral method for solving sparse, unsymmetric linear systems.[48] All simulations were carried out on a Dell Precision WorkStation T7500 with Intel® Xeon® CPU X5670 @2.93 GHz equipped with 24 GB of RAM, with a typical solution time of 1200 s.

Analysis of simulation results

Results of individual simulations are used to characterize the performance of the membrane system for achieving carbon monoxide removal from hydrogen-rich reformate mixtures via manipulations of water-gas-shift reaction and diffusion. The reactor performance is evaluated in terms of an overall conversion of carbon monoxide, defined as

$$X_{\text{CO}} = \frac{F^F_{\text{CO,o}} - \left(F^F_{\text{CO},e} + F^S_{\text{CO},e}\right)}{F^F_{\text{CO},o}} \tag{9}$$

The performance of the catalytic membrane reactor for gas purification is characterized in terms of hydrogen recovery and apparent gas permselectivities. Apparent H_2:CO and H_2:CO_2 permselectivities are defined in terms of molar flows of each species entering the retentate volume and exiting the permeate volume. It is important to differentiate apparent permselectivities from the innate permselectivity arising from the assumption of Knudsen diffusion. The latter is obtained via Eq. 4b as the square root of the ratio of undesired to desired permeate molecular weights, such that the innate Knudsen permselectivity of H_2:CO and H_2:CO_2 are 3.71 and 4.69, respectively. The presence of appropriately manipulated reaction-diffusion phenomena results in significantly higher apparent permselectivities than Knudsen values, as will be shown below.

Apparent selectivities are evaluated for two distinct modes of operation (Figure 2a, b), specifically (i) as a gas purification membrane (GPM), such that selectivities are determined from permeate gas composition, and (ii) as a catalytic reactor (CMR), such that analysis is based on overall, or blended, outlet composition

$$S^{\text{GPM}}_{\text{H}_2/\text{CO}} = \left(\frac{F^S_{\text{H}_2,e}}{F^S_{\text{CO},e}}\right)\Big/\left(\frac{F^F_{\text{H}_2,o}}{F^F_{\text{CO},o}}\right),\ \text{and } S^{\text{GPM}}_{H_2/\text{CO}_2} = \left(\frac{F^S_{\text{H}_2,e}}{F^S_{\text{CO}_2,e}}\right)\Big/\left(\frac{F^F_{\text{H}_2,o}}{F^F_{\text{CO}_2,o}}\right) \tag{10a}$$

$$S^{\text{CMR}}_{\text{H}_2/\text{CO}} = \left(\frac{F^S_{\text{H}_2,e}+F^F_{\text{H}_2,e}}{F^S_{\text{CO},e}+F^F_{\text{CO},e}}\right)\Big/\left(\frac{F^S_{\text{H}_2,o}+F^F_{\text{H}_2,o}}{F^S_{\text{CO},o}+F^F_{\text{CO},o}}\right),$$

$$\text{and } S^{\text{CMR}}_{\text{H}_2/\text{CO}_2} = \left(\frac{F^S_{\text{H}_2,e}+F^F_{\text{H}_2,e}}{F^S_{\text{CO}_2,e}+F^F_{\text{CO}_2,e}}\right)\Big/\left(\frac{F^S_{\text{H}_2,o}+F^F_{\text{H}_2,o}}{F^S_{\text{CO}_2,o}+F^F_{\text{CO}_2,o}}\right) \tag{10b}$$

Two additional reference cases, corresponding to infinite packed-bed reactors (PBRs) supplied with (I) the retentate feed stream, and (II) both retentate and permeate feed streams, are considered for the purpose of comparing apparent permselectivities achieved by the catalytic membrane reactor against values achieved by allowing water-gas-shift reaction to reach chemical equilibrium. The resulting PBR apparent permselectivities are defined as

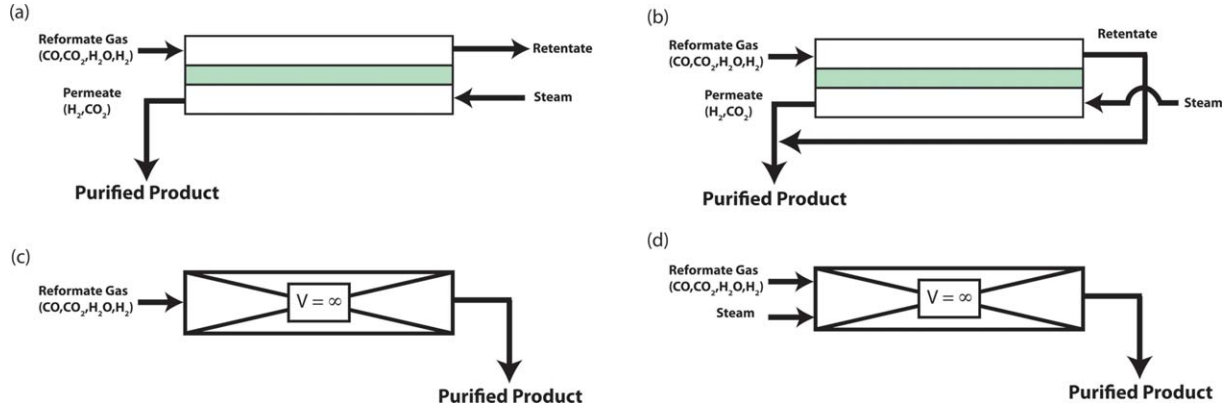

Figure 2. Summary of two membrane reactor modes of operation, (a) gas purification membrane or GPM mode wherein only permeate effluent is retained as the purified product, and (b) catalytic membrane reactor or CMR mode of operation wherein permeate and retentate effluents are blended to form the purified product, and two reference cases of (c) an infinite packed-bed reactor receiving retentate inlet, and (d) an infinite packed-bed reactor receiving mixture of retentate and sweep inlet.

[Color figure can be viewed in the online issue, which is available at wileyonlinelibrary.com.]

$$S^{\mathrm{I,II}}_{\mathrm{H_2/CO}} = \left(\frac{F^{\mathrm{I,II}}_{\mathrm{H_2},o} + X^{\mathrm{I,II}}_{\mathrm{CO},eq}\cdot F^{\mathrm{I,II}}_{\mathrm{CO},o}}{F^{\mathrm{I,II}}_{\mathrm{CO,o}} - X^{\mathrm{I,II}}_{\mathrm{CO},eq}\cdot F^{\mathrm{I,II}}_{\mathrm{CO},o}}\right)\Bigg/\left(\frac{F^{\mathrm{I,II}}_{\mathrm{H_2},o}}{F^{\mathrm{I,II}}_{\mathrm{CO,o}}}\right) = 2.19\ \&\ 10.22\ \text{ at } 773\mathrm{K} \quad (10c)$$

$$S^{\mathrm{I,II}}_{\mathrm{H_2/CO_2}} = \left(\frac{F^{\mathrm{I,II}}_{\mathrm{H_2},o} + X^{\mathrm{I,II}}_{\mathrm{CO},eq}\cdot F^{\mathrm{I,II}}_{\mathrm{CO},o}}{F^{\mathrm{I,II}}_{\mathrm{CO_2,o}} + X^{\mathrm{I,II}}_{\mathrm{CO},eq}\cdot F^{\mathrm{I,II}}_{\mathrm{CO},o}}\right)\Bigg/\left(\frac{F^{\mathrm{I,II}}_{\mathrm{H_2},o}}{F^{\mathrm{I,II}}_{\mathrm{CO_2,o}}}\right) = 0.48\ \&\ 0.35\ \text{ at } 773\mathrm{K} \quad (10d)$$

Last, the percentage of total hydrogen recovered is determined from the outlet molar flows of hydrogen, thus accounting for both hydrogen supplied to the membrane for purification and the potential hydrogen to be produced via water-gas-shift

$$\mathrm{HR} = \frac{F^{S}_{\mathrm{H_2},e}}{F^{F}_{\mathrm{H_2},e} + F^{S}_{\mathrm{H_2},e}} \times 100\% \quad (11)$$

The above metrics provide a fair comparison of the present catalytic membrane design to traditional catalytic membrane and PBR designs for the purpose of CO removal from reformate mixtures.

Results and Discussion

Analysis of CMR performance at $\xi = 0.1$, $\Phi = 7.6$

Simulations were first carried out for the design case corresponding to $\xi = 0.1$, $\Phi = 7.6$ at 773 K. This initial design conditions are selected as a first approximation to establish the design criteria and provide insight into further parametric analysis. Thiele modulus of 7.6 corresponds to an estimated 99.9% of theoretical maximum modification of species partial pressure via reaction at the centerline, while the separation factor is selected such that water-gas-shift reaction is the dominant phenomena within the membrane system. Figure 3 presents the overall carbon monoxide conversion achieved in the catalytic membrane reactor as a function of Damkohler number, Da. The equilibrium carbon monoxide conversion corresponding to feed (reformate) composition $\left(X^{\mathrm{I}}_{\mathrm{CO,Eq}} = 0.474\right)$ and a blend of reformate and sweep gases $\left(X^{\mathrm{II}}_{\mathrm{CO,Eq}} = 0.875\right)$ are provided for reference. As Da increases from zero, carbon monoxide conversion rapidly increases toward the upper limit of $X^{\mathrm{II}}_{\mathrm{CO,Eq}}$, followed by a moderate reduction in conversion with further increases in Da before returning to the upper limit of $X^{\mathrm{II}}_{\mathrm{CO,Eq}}$. This local reduction in CO conversion at intermediate values of Da is the result of axial mass dispersion within the catalytic film which dilutes the driving force for water-gas-shift reaction. This is illustrated in Figure 4, which presents contour maps of CO and H_2O partial pressures at increasing values of Da. Inspection of volume integrals and maximum values of water-gas-shift rates confirm a reduction of overall reaction rate owing to increased diffusive mixing at intermediate values of Da. Figure 3 also identifies a first operating point (†) at which carbon monoxide conversion within the catalytic membrane reactor is equal to the equilibrium conversion corresponding to the reformate composition ($X^{\mathrm{I}}_{\mathrm{CO,Eq}}$). Thus, at operating point (†), the CO conversion achieved by the catalytic membrane reactor is equal to that expected for reference Case II.

Figure 5a presents H_2:CO apparent permselectivities based on the permeate effluent composition for the design case of $\xi = 0.1$, $\Phi = 7.6$ at 773 K. At very high flow rates (i.e., Da approaching zero), catalytic contributions to gas separation become negligible such that observed H_2:CO selectivity is equal to the inherent permselectivity of the catalytic film

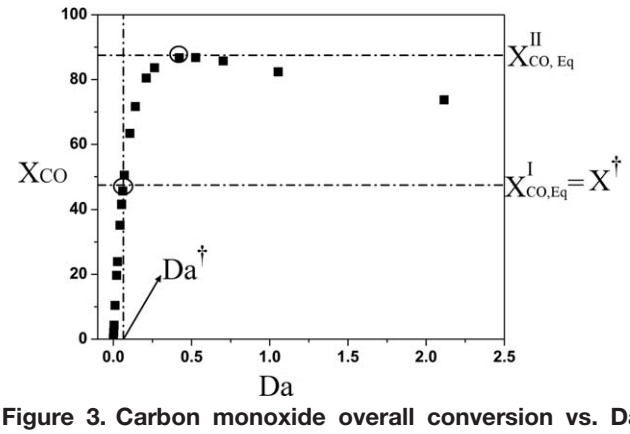

Figure 3. Carbon monoxide overall conversion vs. Da for water-gas-shift catalytic membrane reactor at $\Phi = 7.6$, $\xi = 0.1$.

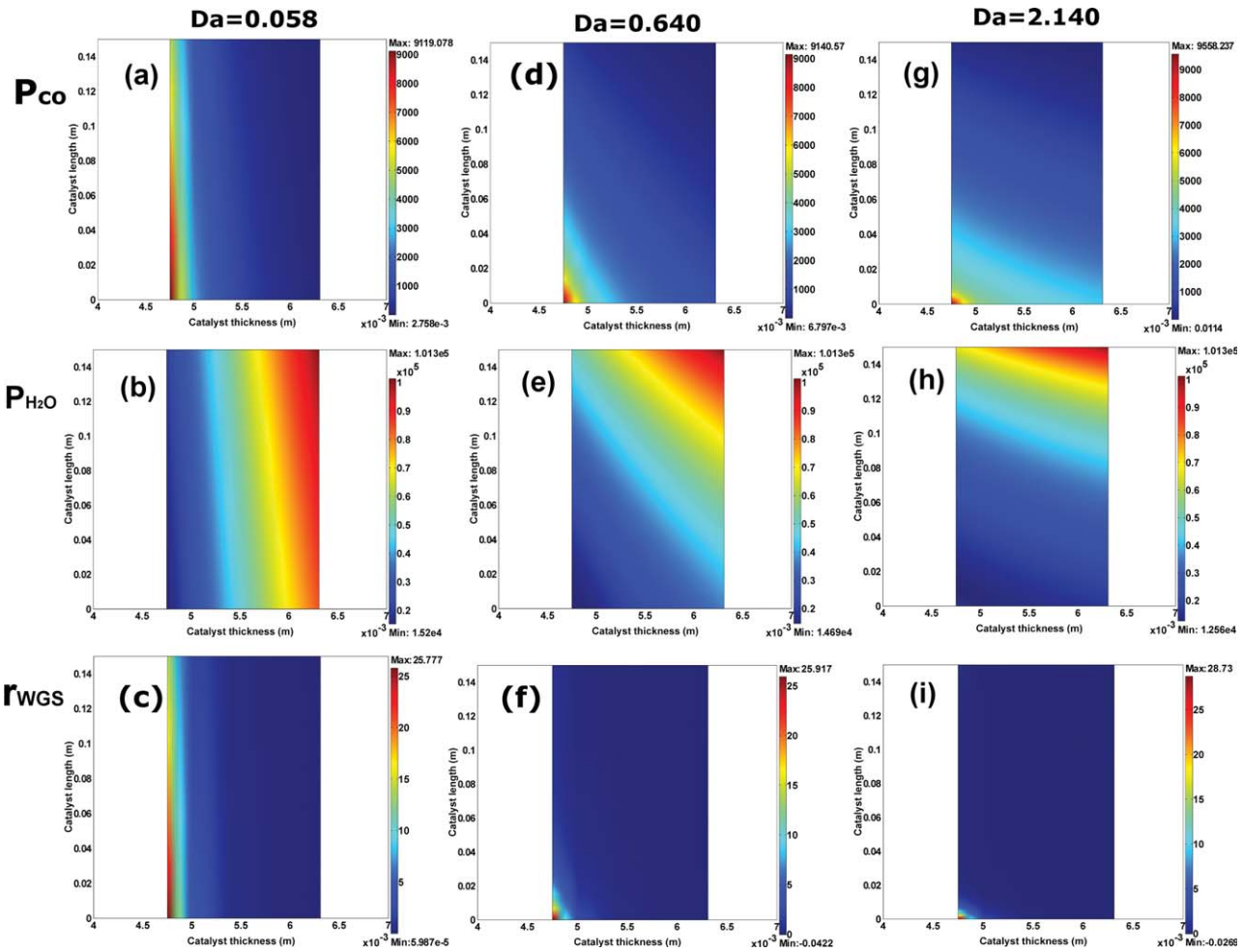

Figure 4. Influence of increasing residence time on mixing in the catalytic membrane, $\Phi = 7.6$, $\xi = 0.1$.

At (a–c) Da = 0.058, (d–f) 0.640 and (g–i) 2.140, (a,d,g) CO partial pressure, (b,e,h) H_2O partial pressure, and (c,f,i) local rate of water-gas-shift reaction are plotted as function of position within the catalytic membrane.

(~3.7:1). Slight increases in Da result in significant increases of apparent H_2:CO permselectivity to a maximum value of 459:1 (shown in inset), followed by an asymptotic decline in selectivity toward the intrinsic Knudsen selectivity of the membrane $\left(S^K_{H_2/CO} = 3.7\right)$ as Da approaches infinity. A second operating point (**) is identified corresponding to this maximum in achievable H_2/CO separation. Figure 5a further allows identification of a third operating point (*), corresponding to $S^{II}_{H_2/CO} = 10.22{:}1$ at 773 K. This third operating point (*) thus represents the maximum Da at which the catalytic membrane reactor is capable of achieving greater CO mitigation in the product stream than a conventional PBR. Figure 5b presents the blended H_2:CO apparent permselectivity as a function of Da. The observed trend in blended permselectivity matches that for carbon monoxide conversion, with a local maximum approaching the aforementioned limit of 10.22:1 coinciding with a maximum conversion approaching the upper limit of $X^{II}_{CO,Eq} = 0.875$.

Figure 6 presents the apparent H_2:CO_2 permselectivities based on permeate effluent composition (GPM) and a blended composition of both retentate and permeate streams (CMR). In both cases, apparent permselectivities are consistently <1:1, owing to the generation of additional carbon dioxide via water-gas-shift reaction. It should be noted, however, that the gas purification mode of operation (i.e., H_2:CO_2 permselectivity based on permeate gas composition) results in a higher ratio of H_2:CO_2 product partial pressures, as compared to the catalytic membrane reactor mode of operation (i.e., H_2:CO_2 permselectivity based on blended effluent composition).

Figure 7 summarizes the performance of the catalytic membrane system for gas purification by directly comparing H_2 recovery and apparent H_2:CO selectivity. The resulting curve is bounded by the intrinsic Knudsen permselectivity of the catalytic film (3.7:1) both as Da approaches zero (corresponding to HR approaching zero), and at Da approaching infinity, corresponding to HR = 66%. The three operating points identified in Figures 3 and 5 provide appropriate boundaries for identifying (i) an unfavorable region of operating space wherein greater removal of CO may be achieved using a conventional PBR, (ii) a region of high CO removal at the expense of low H_2 recovery, and (iii) an intermediate region achieving a combination of favorable CO removal and H_2 recoveries. Based on this analysis, an "optimal" operating point (†), corresponding to an overall CO conversion equal to the equilibrium conversion achievable with the reformate composition (i.e., $@X = X^{I}_{Eq}$), is selected as the most appropriate operating point for employing the catalytic membrane reactor as a GPM. For the case of $\xi = 0.1$ and $\Phi = 7.6$, this design point corresponds to a hydrogen recovery of 24.3% at an apparent H_2:CO permselectivity of 94.7:1.

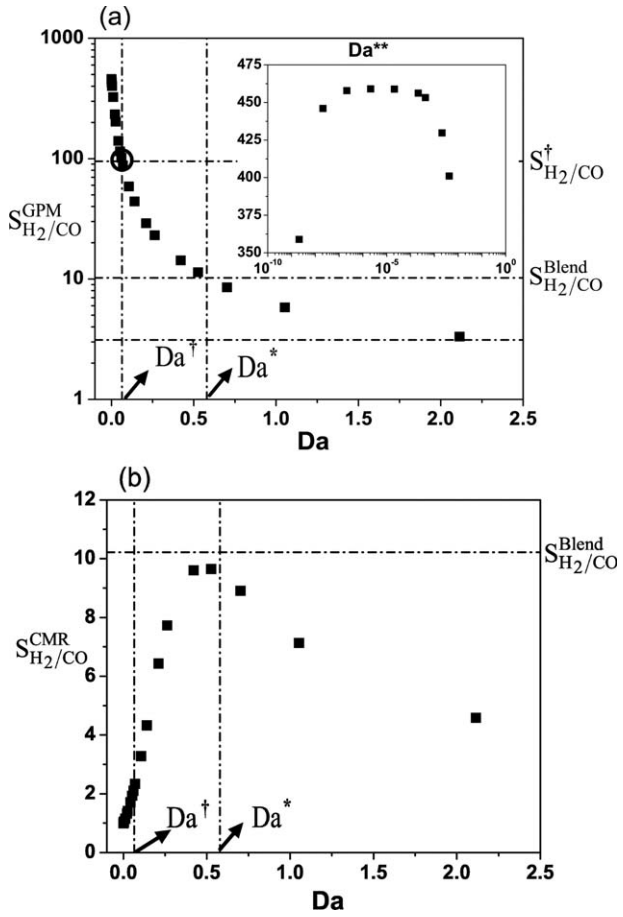

Figure 5. Apparent H_2:CO permselectivity based on (a) permeate effluent composition, and (b) blended composition of retentate and permeate streams presented as a function of Da at $\Phi = 7.6$, $\xi = 0.1$.

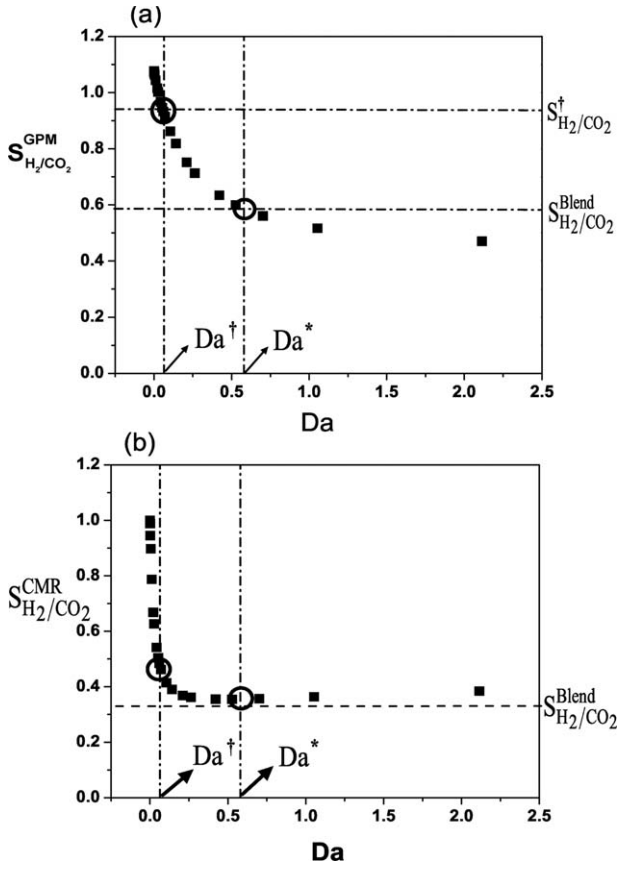

Figure 6. Apparent H_2:CO_2 permselectivity based on (a) permeate effluent composition, and (b) blended composition of retentate and permeate streams presented as a function of Da at $\Phi = 7.6$, $\xi = 0.1$.

Comparison of CMR performance, varying ξ *at* $\Phi = 7.6$

The above analysis is repeated for a sequence of membrane designs (summarized in Table 1) spanning separation factor (ξ) values of 0.1 to 10 while maintaining a constant value for Φ of 7.6. For each membrane design, performance is evaluated at each of the three design points discussed in Section Comparison of CMR performance, varying Φ at $\xi = 0.1$. Figure 8a presents the apparent H_2:CO permselectivity obtained under GPM mode of operation as a function of separation factor, ξ. Two distinct regions ($\xi < 0.4$, and $\xi > 0.5$) are observed for the operating points corresponding to (**) a maximum in H_2:CO apparent permselectivity and (†) the aforementioned "optimal" operating point. Starting at the lowest value of $\xi = 0.1$, negligible loss in permselectivity is initially observed with increasing ξ (increasing the hydrogen permeance relative to rate of water-gas-shift and/or carbon monoxide permeance) up to a limit of $\xi < 0.4$. At values of $\xi > 0.5$, apparent permselectivities are significantly reduced. For the case of the (*) operating point corresponding to CO removal by an infinite PBR, selectivity remains constant as the latter value is not a function of ξ. Figure 8b presents the percentile hydrogen recovery as a function of ξ for all three operating points. For the case of (*) and (†) operating points, slight increases in hydrogen recovery are observed with increasing ξ, which reflects a relative increase in hydrogen permeability. For the case of (**) operating point, a significant increase in hydrogen recovery is observed between $0.4 < \xi$ and $\xi < 0.5$, coinciding with a drop-off in corresponding maximum H_2:CO apparent permselectivity (Figure 6a). Overall, the results presented in Figure 8 confirm that the best gas purification performance is achieved by the (†) operating point under conditions wherein $\xi < 0.4$.

The results in Figure 8 therefore indicate an upper limit in pore diameter, beyond which this approach to gas

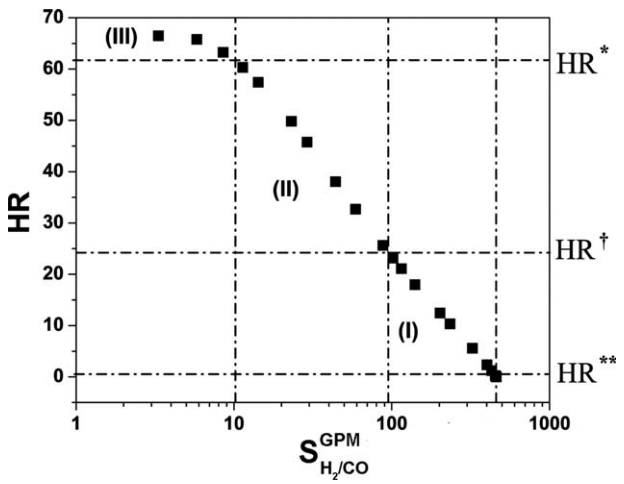

Figure 7. H_2 recovery vs. effective H_2:CO permselectivity, $\Phi = 7.6$, $\xi = 0.1$.

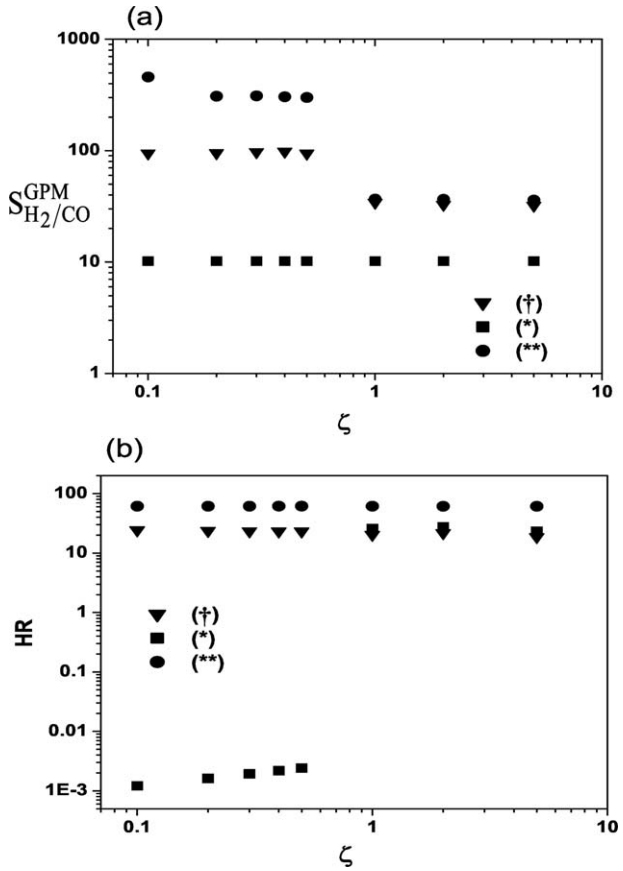

Figure 8. Comparison of membrane design performance at $\Phi = 7.6$.

(a) Apparent H_2:CO permselectivity based on permeate effluent composition as function of ξ; (b) H_2 recovery (HR) as function of ξ.

separations becomes ineffective. Recognizing that Figure 8a imposes the design criteria of a fixed value for Φ, combination of Eqs. 1 and 4b indicates that the target membrane thickness scales with the square root of the pore diameter. Substitution into Eq. 2 thus indicates that the separation factor increases with the square root of the pore diameter as well. Thus, for a specific application, there is expected to be a maximum allowable pore diameter beyond which a value of $\xi < 0.4$ is unattainable at a desirable value of Φ.

Comparison of CMR performance, varying Φ at $\xi = 0.1$

Analysis is repeated for a sequence of membrane designs (summarized in Table 1) spanning normalized Thiele moduli (Φ) of 7.6–1 while maintaining a constant value of $\xi = 0.1$, in terms of the three operating points discussed above. Figure 9a presents the influence of decreasing Thiele moduli on apparent H_2:CO selectivity at each operating point. As discussed above, the selectivity corresponding to an infinite packed bed (*) is invariant to the catalytic membrane design. The maximum (**) apparent selectivity decreases to a value of 10.2 (corresponding to the aforementioned reference case of an infinite packed bed) as Φ approaches unity, while the apparent selectivity corresponding to the (†) operating point falls below this minimum value at $\Phi < 1.5$.

Figure 9b presents the influence of decreasing Thiele moduli (Φ) on hydrogen recovery at $\xi = 0.1$. Increasing trends in hydrogen recovery are observed for both (†) and (**) operating points, which indicates that as Thiele moduli is decreased, lower selectivities are achievable by the membrane as the impact of water-gas-shift reaction on gas composition is reduced. This in turn alleviates the need for maintaining high-concentration gradients across the membrane via low residence times (or values of Da), which limits hydrogen recovery rates. Thus, decreasing Thiele moduli results in poor maximum selectivities, which may nevertheless be achieved at higher residence times and therefore greater hydrogen recovery rates. Overall, the results in Figure 9 indicate that a design criteria of $\Phi = 7.6$ is sufficient to achieve high permselectivities for both (†) and (**) operating points, whereas further increases in Thiele moduli represent a diminishing return on selectivity at the cost of further reduction in recovery rates.

Comparison of isothermal CMR performance, varying temperature

Based on the above analysis, a design point of ($\Phi = 7.6$, $\xi = 0.1$) and the (†) operating point are selected as a basis for comparing catalytic membrane performance for gas purification over a range of five isothermal operating temperatures. Figure 10 shows the permeate hydrogen recovery as a function of apparent H_2:CO permselectivity obtained over a range of Da at each isothermal operating temperature studied. In all cases, hydrogen recovery and H_2:CO permselectivity follow the same trend discussed in Section Comparison of CMR performance, varying Φ at $\xi = 0.1$. Permeate

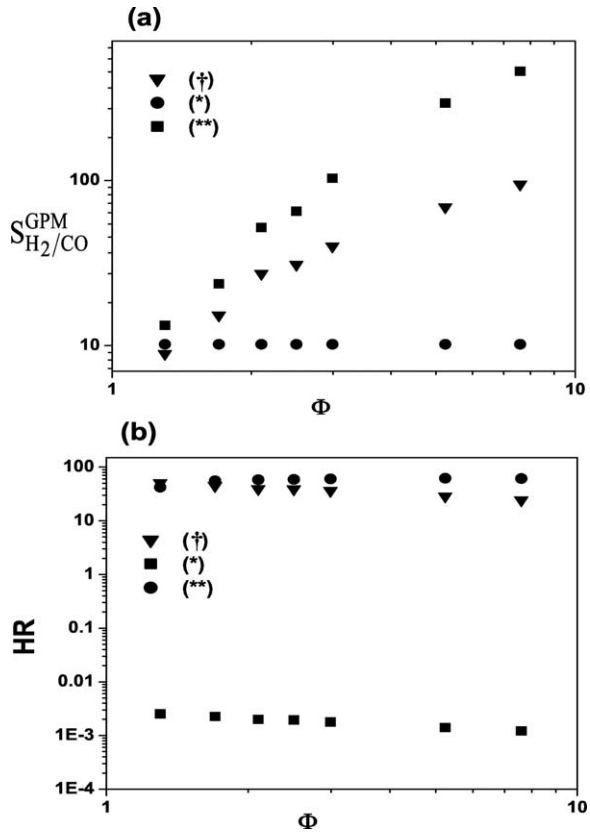

Figure 9. Comparison of membrane design performance at $\xi = 0.1$.

(a) Apparent H_2:CO permselectivity based on permeate effluent composition as function of Φ, (b) H_2 recovery (HR) as function of Φ.

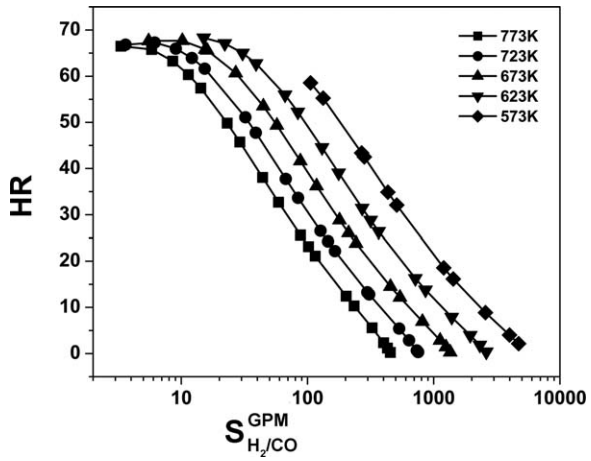

Figure 10. Comparison of GPM design performance as function of temperature at corresponding Damkohler number.

H_2 recovery (HR) vs. effective H_2:CO permselectivity, $\Phi = 7.6$, $\xi = 0.1$.

hydrogen recovery and apparent H_2/CO separation increase with decreasing temperature as reaction equilibrium shifts toward CO_2 and H_2 formation.

Table 2 summarizes both membrane dimensional design parameters (t, δ) and performance in terms of hydrogen recovery and apparent selectivities achieved by GPM operation mode over the range of isothermal operating temperatures studied. The corresponding selectivities for the two infinite PBR cases are provided for comparison. Results indicate that as reaction temperature decreases, the achievable H_2:CO permselectivity increases owing to removal of equilibrium limitations on the catalytic conversion of CO to CO_2. As reaction rates decrease with temperature, the residence time necessary to achieve sufficient reaction for design point (†) increases, which corresponds to an increase in hydrogen recovery rate. Thus, as temperature is decreased, both the H_2:CO apparent selectivity and H_2 recovery rate are improved.

Further details of the (†) operating point for the design case of (573 K, $\Phi = 7.6$, $\xi = 0.1$) are presented to provide additional assessment of this novel application of catalytic membranes to gas purification. For a catalytic membrane of 5.67-mm thickness and catalyst activity factor (δ) of 0.30, the apparent H_2:CO permselectivity is 298.4:1 at a H_2 recovery rate of 41.6%, with corresponding feed and effluent compositions summarized in Table 3. The permeate gas produced with above conditions has a CO content of 0.022% and H_2 content of 20.6%, or 0.06% CO and 58% H_2 on a dry-gas basis. For a single-tube-and-shell membrane with inner radius of 4.75 mm, outer radius of 10.42 mm, and length of 150 mm, these conditions correspond to a feed (reformate) molar flow rate of 5.15×10^{-5} mol s^{-1} and sweep (steam) molar flow rate of 3.4×10^{-6} mol s^{-1} (Da = 0.1) at a hydrogen flux across the membrane of 8.49×10^{-4} mol H_2 per m^2 of membrane, or 0.038 mol H_2/s per Kg of catalyst/membrane. This value is significantly lower than membrane reactors detailed in the literature, indicating that the present design is not efficient from a reactor design perspective. However, from the perspective of a hydrogen purification membrane, these results are shown to be quite promising.

Table 2. Summary of Design Parameters and Results for Varying T at $\Phi = 7.6$, $\xi = 0.1$

T (K)	t (m)	δ	$S_{H_2/CO}$	S_{H_2/CO_2}	R (%)
773.15	1.56×10^{-3}	0.23	94.7:1	0.92:1	24.3
723.15	2.07×10^{-3}	0.25	112.7:1	0.9:1	27.3
673.15	2.78×10^{-3}	0.28	136.3:1	0.87:1	31.0
623.15	3.88×10^{-3}	0.32	215:1	0.83:1	35.2
573.15	5.67×10^{-3}	0.35	298.4:1	0.76:1	41.6

Hydrogen compositions entering and exiting both permeate and retentate volumes allow determination of a log-mean driving force as follows

$$\text{LMPD} = \frac{\Delta P^a_{H_2} - \Delta P^b_{H_2}}{\ln\left[\frac{\Delta P^a_{H_2}}{\Delta P^b_{H_2}}\right]}, \quad \text{where } \Delta P^a_{H_2} = P^{\text{Retentate}}_{H_2,\text{in}} - P^{\text{Permeate}}_{H_2,\text{out}} \text{ and } \Delta P^a_{H_2} = P^{\text{Retentate}}_{H_2,\text{out}} - P^{\text{Permeate}}_{H_2,\text{in}} \tag{12}$$

Effluent compositions summarized in Table 3 correspond to an log-mean differential pressure of 20,000 Pa, which combined with a membrane thickness of 5.59 mm yields an apparent hydrogen permeability of 2.37×10^{-10} mol m^{-1} Pa^{-1} s. This value compares favorably against that of palladium membranes, which are capable of typical hydrogen permeability of $\sim 2 \times 10^{-11}$ mol m^{-1} Pa^{-1} s.[14,49]

Adiabatic operation: Influence of reaction heat and imposed thermal gradients

The performance of the catalytic membrane for gas purification was investigated under adiabatic conditions to ascertain the impact of reaction heat accumulation on gas purification. Solutions to the adiabatic membrane reactor model detailed in Section Model assembly were obtained over a range of reactor Damkohler number for a membrane design corresponding to $\xi = 0.1$ and $\Phi = 7.6$ at 773 K. Three adiabatic cases were studied; (i) membrane operation with matched feed and sweep inlet temperatures of 773 K, (ii) membrane operation with feed and sweep temperatures of 890 and 623 K, respectively, and (iii) membrane operation with feed and sweep temperatures of 679 and 930K, respectively. For the latter two cases, temperatures were selected such that the normalized temperature gradient, ψ was ~ 0.3[50] while ensuring an averaged inlet temperature of 773 K, as calculated from Eq. 14

$$\psi = \frac{T^F_o - T^S_o}{T^F_o} \text{ for adiabatic case (ii) and } \psi = \frac{T^S_o - T^F_o}{T^S_o} \text{ for adiabatic case (iii)} \tag{13}$$

$$T_{\text{ave}} = \frac{\left(C_{p,F} \cdot F^F_o \cdot T^F_o + C_{p,S} \cdot F^S_o \cdot T^S_o\right)}{\left(C_{p,F} \cdot F^F_o + C_{p,S} \cdot F^S_o\right)} \tag{14}$$

Figure 11a presents a comparison of overall carbon monoxide conversion obtained for isothermal operation with the

Table 3. Summary of Design Point (†) Performance in Terms of Mole Fractions at 573 K, $\Phi = 7.6$ and $\xi = 0.1$

	Feed (−)	Retentate (−)	Sweep (−)	Permeate (−)
y_{CO}	0.09	1.31×10^{-2}	0.0	2.22×10^{-4}
y_{CO_2}	0.03	9.25×10^{-2}	0.0	2.89×10^{-2}
y_{H_2}	0.28	2.23×10^{-1}	0.0	2.06×10^{-1}
y_{H_2O}	0.15	2.84×10^{-1}	1.0	6.45×10^{-1}

three adiabatic cases described above. Results show that overall carbon monoxide conversion for all four cases follow the trend previously described in Section Comparison of CMR performance, varying Φ at $\xi = 0.1$. A comparison of membrane apparent H_2:CO permselectivity for the isothermal and adiabatic cases (Figure 11b) indicates H_2:CO permselectivities obtained from isothermal operation are higher than the adiabatic case of uniform inlet temperatures. Operation with an externally imposed, sweep-to-feed thermal gradient further reduces achievable H_2:CO apparent permselectivity, whereas an externally-induced feed-to-sweep thermal gradient reduces the loss in apparent selectivity from adiabatic operation. A comparison of hydrogen recoveries (Figure 11c) indicates a negligible effect of nonisothermality on hydrogen transport rates. These trends combine to indicate a shift in H_2:CO selectivities with negligible change in recovery rates when reaction heat produced by the equilibrium-limited water-gas-shift reaction is allowed to accumulate within the membrane reactor. Simulations indicate that this negative impact of reaction heat accumulation may be partially mitigated by imposition of an opposing thermal gradient.

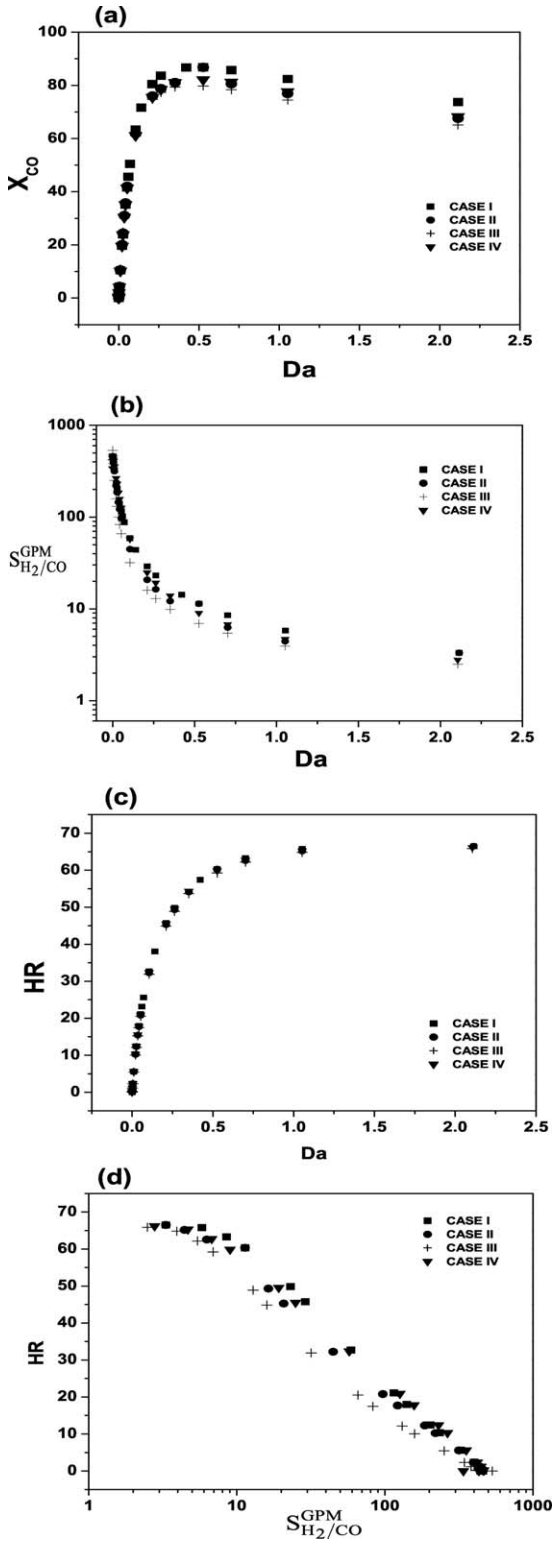

Figure 11. Comparison of GPM design performance as function of temperature at corresponding Damkohler number.

(a) CO conversion (b) apparent permselectivity of H_2/CO based on permeate effluent composition (c) H_2 recovery (HR) (d) apparent permselectivity of H2/CO vs H_2 recovery, at $\xi = 0.1$.

Conclusions

The authors have explored a novel application for a catalytic membrane reactor, specifically for achieving selective removal of CO from H_2-rich reformate mixtures solely by manipulation of reaction and diffusion phenomena, that is, without employing any permselective materials. In this application, a typical reformate mixture (9% CO, 3% CO_2, 28% H_2, and 15% H_2O) is supplied to the retentate volume of a tube-and-shell membrane reactor, whereas pure steam is supplied to the permeate volume such that the overall H_2O:CO ratio within the system is 9:1. Simulations indicate that apparent CO:H_2 selectivities of 90:1 to >200:1 at H_2 recoveries of 20% to upwards of 40% may be achieved through appropriate design of the catalytic membrane and selection of operating conditions. Two design criteria are identified for achieving selective removal of CO from H_2-rich reformate mixtures, in terms of the catalytic film Thiele moduli ($\Phi = 7.6$) and a dimensionless ratio of H_2 permeation to CO conversion rates ($\xi < 0.4$). A methodology for identifying a suitable range of operating parameters is presented, based on a target operating point corresponding to a CO conversion equal to the equilibrium conversion calculated using the reformate feed composition. At an isothermal membrane reactor temperature of 573K corresponding to a catalytic membrane thickness of 5.67×10^{-3}, this operating point results in a H_2:CO apparent permselectivity of 298.4:1 at a H_2 recovery of 41.6%; permeate gas produced under these conditions has a CO content of 0.022% and H_2 content of 20.6%, or 0.06% CO and 58% H_2 on a dry-gas basis. Comparison of adiabatic and isothermal simulations indicates that accumulation of reaction heat reduces apparent permselectivities; however, this may be mitigated by external imposition of a countering thermal gradient.

Acknowledgments

This work was supported by National Science Foundation CAREER Award #0748016 administered by the Process and Reaction Engineering Program. Additional support was provided through a Young Faculty Award from the DuPont De Nemours Coorporation and the Artie McFerrin Department of Chemical Engineering at Texas A&M University. The authors are also indebted to Mr. Jeff Polasek and Mr. Joel

James for providing technical support and computing resources.

Notation

$\hat{a}^{F,S}$ = ratio of membrane surface area to fluid volume (m^{-1})
$A_C^{F,S}$ = cross sectional area for flow (m^2)
A_{mem} = membrane surface area (m^2)
C_i = concentration of species i (mol m^{-3})
$C_{p,F}$ = specific heat capacity of retentate gas mixture (J mol^{-1} K^{-1})
$C_{p,S}$ = specific heat capacity of permeate gas mixture (J mol^{-1} K^{-1})
d_p = catalyst pore diameter (m)
$D_{i,K}^{eff}$ = Knudsen diffusivity of species i (m^2 s^{-1})
Da = Damkohler number (dimensionless)
$F_i^{F,S}$ = molar flow rate of species i (mol s^{-1})
h^S = fluid-wall heat-transfer coefficient (J m^{-2} s^{-1} K^{-1})
h^F = fluid-wall heat-transfer coefficient (J m^{-2} s^{-1} K^{-1})
HR = hydrogen recovery in sweep (%)
k_f = forward rate coefficient of reaction (mol m^{-3} s^{-1} Pa^{-2})
k_c = effective thermal conductivity of catalyst
k_{cat} = thermal conductivity of catalyst (J m^{-1} s^{-1} K^{-1})
k_{gas} = thermal conductivity of gas mixture (J m^{-1} s^{-1} K^{-1})
k_{gs} = mass-transfer coefficient at gas-solid interface (mol m^{-2} s^{-1})
k_{solid} = thermal conductivity of solid (J m^{-1} s^{-1} K^{-1})
K_{eq} = equilibrium coefficient for water-gas-shift reaction (dimensionless)
M_i = molecular weight of species i (kg mol^{-1})
L = membrane length (m)
$\tilde{n}$ = normal surface vector (dimensionless)
p_i = partial pressure of species i (Pa)
P = reactor total pressure (Pa)
r_{CO} = rate of carbon monoxide in WGS reaction (mol m^{-3} s)
r_i = rate of appearance for species i via WGS reaction (mol m^{-3} s)
R = universal gas constant (J mol^{-1} K^{-1})
$S_{i/j}$ = apparent permselectivity of species i over species j
t_{mem} = catalyst thickness (m)
t_{cat} = catalyst thickness (m)
T = temperature (K)
T^{cat} = temperature (K)
T^F = feed volume temperature (K)
T^S = sweep volume temperature (K)
T_{ave} = inlet average temperature of feed and sweep (K)
T_o^F = initial temperature of retentate volume (K)
T_o^S = initial temperature of permeate volume (K)
V_{mem} = membrane volume (m^3)
$V^{F,S}$ = flow volume (m^3)
w_i = mass fraction of species i (dimensionless)
X_i = fractional conversion of species i (dimensionless)
x_j = mole fraction of species i (dimensionless)

Greek letters

δ = catalyst activity factor (dimensionless)
ΔH_{rxn}^o = heat of WGS reaction (J mol^{-1})
η = catalyst effectiveness factor (dimensionless)
Φ = modified Thiele modulus (dimensionless)
μ_i = viscosity of pure species i, (Pa s)
μ_g = viscosity of gas mixture (Pa s)
ε = porosity of catalytic membrane (dimensionless)
ρ = density of gas (m^3 kg^{-1})
σ = Lennard–Jones parameter for determining gas viscosity
Ω_μ = Lennard–Jones parameter for determining gas viscosity
τ = tortuosity factor of catalytic membrane (dimensionless)
ξ = separation factor (dimensionless)
ψ = defined in Eq. 15

Subscripts

CO = carbon monoxide
CO_2 = carbon dioxide
e = exit/outlet condition
H_2 = hydrogen
H_2O = steam
o = initial/inlet condition

Superscripts

cat = catalytic membrane volume
CMR = catalytic membrane reactor mode of operation
F = feed volume
GPM = gas purification membrane mode of operation
PBR = infinite packed bed reactor, reference case
S = sweep volume

Literature Cited

1. Zagoria A, Huycke R. Refinery hydrogen management—the big picture. *Hydrocarb Process*. 2003;82:41–46.
2. Hallale N, Liu F. Refinery hydrogen management for clean fuels production *Adv Environ Res*. 2001;6:81–98.
3. Alves JJ, Towler GP. Analysis of refinery hydrogen distribution systems. *Ind Eng Chem*. 2002;41:5759–5769.
4. Elliott DC. Historical developments in hydroprocessing bio-oils. *Energy Fuels*. 2007;21(3):1792–1815.
5. French RJ, Hrdlicka J, Baldwin R. Mild hydrotreating of biomass pyrolysis oils to produce a suitable refinery feedstock. *Environ Prog Sustain Energy*. 2010;29(2):142–150.
6. Holladay JD, Hu J, King DL, Wang Y. An overview of hydrogen production technologies. *Catal Today*. 2009;139(4):244–260.
7. Haryanto A, Fernando S, Murali N, Adhikari S. Current status of hydrogen production techniques by steam reforming of ethanol: a review. *Energy Fuels*. 2005;19(5):2098–2106.
8. Bernardo P, Drioli E, Golemme G. Membrane gas separation: a review/state of the art. *Ind Eng Chem Res*. 2009;48(10):4638–4663.
9. Baker RW. Future directions of membrane gas separation technology. *Ind Eng Chem Res*. 2002;41(6):1393–1411.
10. Strathmann H. Membrane separation processes: current relevance and future opportunities. *AIChE J*. 2001;47(5):1077–1087.
11. Shao L, Low BT, Chung T-S, Greenberg AR. Polymeric membranes for the hydrogen economy: contemporary approaches and prospects for the future. *J Memb Sci*. 2009;327(1–2):18–31.
12. Lin H, Van Wagner E, Freeman BD, Toy LG, Gupta RP. Plasticization-enhanced hydrogen purification using polymeric membranes. *Science*. 2006;311(5761):639–642.
13. Koros WJ, Fleming GK. Membrane-based gas separation. *J Memb Sci*. 1993;83(1):1–80.
14. Paglieri SN, Way JD. Innovations In Palladium Membrane Research. *Separ Purif Rev*. 2002;31(1):1–169.
15. Zou J, Ho WSW. Hydrogen purification for fuel cells by carbon dioxide removal membrane followed by water gas shift reaction. *J Chem Eng Jpn*. 2007;40(11):1011–1020.
16. Uemiya S, Sato N, Ando H, Kikuchi E. The water gas shift reaction assisted by a palladium membrane reactor. *Ind Eng Chem Res*. 1991;30(3):585–589.
17. Baker RW, Lokhandwala K. Natural gas processing with membranes: an overview. *Ind Eng Chem Res*. 2008;47(7):2109–2121.
18. Ockwig NW, Nenoff TM. Membranes for hydrogen separation. *ChemInform*. 2007;38(50):4078–4110.
19. Israni SH, Harold MP. Methanol steam reforming in Pd−Ag membrane reactors: effects of reaction system species on transmembrane hydrogen flux. *Ind Eng Chem Res*. 2010;49(21):10242–10250.
20. Kim D, Donohue D, Kuncharam B, Duval C, Wilhite BA. Toward an integrated ceramic micromembrane network: effect of ethanol reformate on palladium membranes. *Ind Eng Chem Res*. 2010;49(21):10254–10261.
21. Unemoto A, Kaimai A, Sato K, Otake T, Yashiro K, Mizusaki J, Kawada T, Tsuneki T, Shirasaki Y, Yasuda I. The effect of coexisting gases from the process of steam reforming reaction upon hydrogen permeability of palladium alloy membrane at high temperatures. *Int J Hydrogen Energy*. 2007;32:2881–2887.
22. Shu J, Grandjean BPA, Kaliaguine S, Ciavarella P, Giroir-Fendler A, Dalmon JA. Gas permeation and isobutane dehydrogenation over very thin Pd/ceramic membranes. *Can J Chem Eng*. 1997;75(4):712–720.
23. Lin YS. Microporous and dense inorganic membranes: current status and prospective. *Separ Purif Technol*. 2001;25:39–55.
24. Wei Q, Wang F, Nie Z-R, Song C-L, Wang Y-L, Li Q-Y. Highly hydrothermally stable microporous silica membranes for hydrogen separation. *J Phys Chem B*. 2008;112:9354–9359.
25. Lu GQ, Diniz da Costa JC, Duke M, Giessler S, Socolow R, Williams RH, Kreutz T. Inorganic membranes for hydrogen production and purification: a critical review and perspective. *J Colloid Interf Sci*. 2007;314(2):589–603.

26. Ockwig NW, Nenoff TM. Membranes for hydrogen separation. *Chem Rev*. 2007;107:4078–4110.
27. Sanchez Marcano JG, Tsotsis TT. *Catalytic Membranes and Membrane Reactors*. Weinheim: Wiley-VCH, 2002.
28. Westermann T, Melin T. Flow-through catalytic membrane reactors—principles and applications. *Chem Eng Process*. 2009;48(1):17–28.
29. Champagnie AM, Tsotsis TT, Minet RG, Wagner E. The study of ethane dehydrogenation in a catalytic membrane reactor. *J Catal*. 1992;134(2):713–730.
30. Sun YM, Khang SJ. Catalytic membrane for simultaneous chemical reaction and separation applied to a dehydrogenation reaction. *Ind Eng Chem Res*. 1988;27(7):1136–1142.
31. Veldsink JW, van Damme RMJ, Versteeg GF, van Swaaij WPM. Applications of a non-permselective, catalytically active membrane, a model study. *Chem Eng Commun*. 1998;169(1):145–166.
32. Harold MP, Lee C. Intermediate product yield enhancement with a catalytic inorganic membrane-II nonisothermal and integral operation in a back-mixed reactor. *Chem Eng Sci*. 1997;52(12):1923–1939.
33. Harold MP, Zaspalis VT, Keizer K, Burggraaf AJ. Intermediate product yield enhancement with a catalytic inorganic membrane-I. Analytical model for the case of isothermal and differential operation. *Chem Eng Sci*. 1993;48(15):2705–2725.
34. Sloot HJ, Versteeg GF, Van Swaaij WPM. A non-permselective membrane reactor for chemical processes normally requiring strict stoichiometric feed rates of reactants. *Chem Eng Sci*. 1990;45(8):2415–2421.
35. Veldsink JW, van Damme RMJ, Versteeg GF, van Swaaij WPM. A catalytically active membrane reactor for fast, exothermic, heterogeneously catalysed reactions. *Chem Eng Sci*. 1992;47(9–11):2939–2944.
36. Veldsink JW, Versteeg GF, van Swaaij WPM. A catalytically active membrane reactor for fast, highly exothermic, heterogeneous gas reactions. a pilot plant study. *Ind Eng Chem Res*. 1995;34(3):763–772.
37. Burggraaf AJ, Cot L. Fundamentals of inorganic membrane science and technology. *Elsevier Science*, 1996.
38. Kim D, Barnett K, Wilhite BA. Experimental demonstration of enhanced hydrogen permeation in palladium via a composite catalytic-permselective membrane. *AIChE J*. 2013;59(5):1627–1634.
39. Aris R. The mathematical theory of diffusion and reaction in permeable catalysts, Vol. I & II. Oxford: Clarendon Press, 1975.
40. Carberry JJ. The micro-macro effectiveness factor for the reversible catalytic reaction. *AIChE J*. 1962;8(4):557–558.
41. Wilhite BA. Composite catalytic-permselective membranes: a strategy for enhancing selectivity and permeation rates via reaction and diffusion. *Ind Eng Chem Res*. 2011;50(17):10185–10193.
42. Neurock M, M.Stark S, T.Klein M. Molecular simulation of kinetic interactios in complex mixtures. In: Becker ER, J.Pereira C, editors. *Computer-Aided Design of Catalysts*: Marcel Dekker, Inc., 1993.
43. Mizsey P, Newson E, Truong T-b, Hottinger P. The kinetics of methanol decomposition: a part of autothermal partial oxidation to produce hydrogen for fuel cells. *Appl Catal A Gen*. 2001;213(2):233–237.
44. Butt JB. Thermal conductivity of porous catalysts. *AIChE J*. 1965;11(1):106–112.
45. Dixon AG, Cresswell DL. Theoretical prediction of effective heat transfer parameters in packed beds. *AIChE J*. 1979;25(4):663–676.
46. Wilke CR. A Viscosity Equation for gas mixtures. *J Chem Phys*. 1950;18(4):517–519.
47. Bird RB, Stewart WE, Lightfoot EN. *Transport Phenomena*, *2nd ed*. New York: Wiley, 2006.
48. Davis TA. A column preordering strategy for the unsymmetric-pattern multifrontal method. *ACM Trans Math Softw*. 2004;30(2):165–195.
49. Gallucci F, Fernandez E, Corengia P, van Sint Annaland M. Recent advances on membranes and membrane reactors for hydrogen production. *Chem Eng Sci*. 2013;92:40–66.
50. Romero EL, Wilhite BA. Enhancement of water-gas-shift conversion via externally imposed temperature profiles: comparison of linear, convex and Gaussian profiles. *Chem Eng J*. 2011;175(0):433–442.

Manuscript received Feb. 26, 2013, and revision received Jun. 14, 2013.